

# Microstructural Evolution Behavior of Adiabatic Shear Bands Induced by High-speed Projectile Impact in TC32 Titanium Alloy

Xin Yunpeng, Zhu Zhishou, Wang Xinnan, Li Mingbing, Liu Gechen, Li Jing, Shang Guoqiang, Zhu Liwei

Beijing Institute of Aeronautical Materials, Aero Engine Corporation of China, Beijing 100095, China

**Abstract:** The microstructure characterization and evolution behavior of TC32 titanium alloy after high-speed projectile impact were studied by optical microscope (OM), scanning electron microscope (SEM) and transmission electron microscopy (TEM). The distribution of adiabatic shear band (ASB) and stress around the crater has always been a semi-circular diffusion. The rotating refinement process of large equiaxed grains and elongated lath subgrains in adiabatic shear band is observed. Focus ion beam (FIB) technology was used to accurately prepare TEM samples from the crack tip in the ASB. The coexistence of the amorphous regions, the amorphous-to-crystalline transition regions, the fine-scale nano-crystalline region around the crack tip is found. The calculation proves that the temperature rise in ASB could cause microstructure melting, the amorphous regions and small size nanocrystals form after fast quenching. Because the microstructure in the ASBs is fine equiaxed grains and amorphous with higher strength, the area between the deformed band and matrix is relatively weakened, and it is found that the initiation of cracks in adiabatic shear bands is mainly concentrated at the junction of deformed band and matrix, and the crack propagates in the form of microvoids rotation coupling.

**Key words:** adiabatic shear band; nanocrystal; amorphous; TC32 titanium alloy

Titanium and its alloys have been widely used in aerospace, weapons, ships due to their low density, high specific strength, high corrosion resistance<sup>[1,2]</sup>. TC32 titanium alloy has great potential as aerospace materials due to its low cost and excellent performance. When the alloy is applied in these fields, it often bear high strain rate impact, such as projectile impact. However, due to the low thermal conductivity and high strength of titanium, adiabatic shear failure is prone to occur under the high-strain-rate deformation (HSRD)<sup>[3-5]</sup>. In order to improve the bullet-proof property of TC32 titanium alloy, the adiabatic shear failure behavior needs to be further studied.

When metal or alloy deforms at a high-strain-rate, shear banding is a main deformation mechanism, which is usually considered as an adiabatic shear localization phenomenon.

The narrow and severely deformed white band is also called adiabatic shear band (ASB)<sup>[6-9]</sup>. Even if the cracks do not occur, the cutting effect of ASBs on the matrix is disastrous<sup>[10-13]</sup>. Researchers have conducted a great deal of theoretical and experimental research on the crystal structure and micro-structure in ASBs to understand the formation and development of ASBs<sup>[14-20]</sup>. It is still difficult to observe the evolution of microstructure of materials during HSRD process by the in-situ experiments. The mechanism of microstructure formation in ASB is calculated and inferred based on the experimental results.

Me-Bar et al<sup>[21]</sup> studied the ASBs of Ti-6Al-4V titanium alloys with different microstructure. It was found that the microstructures in the ASBs are the same, all of which are finely transformed phases with arbitrary orientation.

Received date: October 25, 2019

Corresponding author: Zhu Zhishou, Ph. D., Professor, Beijing Institute of Aeronautical Materials, Aero Engine Corporation of China, Beijing 100095, P. R. China, Tel: 0086-10-62496635, E-mail: zhuzzs@126.com

Copyright © 2020, Northwest Institute for Nonferrous Metal Research. Published by Science Press. All rights reserved.

Andrade<sup>[22]</sup> studied the dynamic recrystallization of copper at HSRD, and found equiaxed grains generated by dynamic recrystallization inside the ASBs. Meyers et al<sup>[15,23-25]</sup> proposed a subgrain rotational dynamic recrystallization mechanism to explain the mechanism of microstructure formation in ASBs. It is believed that the dislocation rearrangement causes entanglement and annihilation to form fine equiaxed grains. This mechanism has been used to explain the ASBs of metals such as copper<sup>[18]</sup>, zirconium<sup>[26]</sup>, and tantalum<sup>[27]</sup>. At the same time, this study believes that the existence of nano-grains is caused by dynamic recrystallization, and at the first time they have observed amorphous transformation inside the ASBs, but these studies cannot explain the existence of nanocrystalline (<10 nm) and amorphous. The key to determine the mechanism of microstructural evolution in ASBs is whether the adiabatic temperature rise caused by HSRD can lead to melting, which is still an open question and there is no unified conclusion. For the microcracks which formed in the ASBs, Timothy and Hutchings<sup>[28-30]</sup> proposed a mechanism that the cracks are originated from the microvoids and rotate under the action of shear stress to form cracks. Therefore, it is necessary to further understand the microstructure evolution behavior and crack formation in adiabatic shear band, so as to contribute to improving the bullet-proof property of TC32 titanium alloy.

In this study, TC32 titanium alloy was used as the research object to study the microstructural evolution behavior in the ASBs after being impacted by high-speed projectiles. The phenomenon of subgrain rotational dynamic recrystallization, and the microstructure in ASBs were analyzed. It has been found that the large amorphous regions and nanocrystals of different sizes (5~100 nm) formed in the crack tip region in the adiabatic shear band, indicating that high-speed impact can lead to a melting-fast quenching process in the adiabatic shear band. And the existence of fine equiaxed crystals and amorphous in ASBs caused cracks to initiate at the junction of deformed band and matrix.

## 1 Experiment

### 1.1 Experimental materials

TC32 titanium alloy is a new type of low-cost titanium alloy provided by Beijing Institute of Aeronautical Materials, Aero Engine Corporation of China. The forged TC32 titanium alloy sheet was solution treated at 1143 K for 2 h, and then it was air cooled. Aging treatment was conducted on the solution treated sheet at 923 K for 4 h and then air cooled. As shown in Fig.1, the microstructure of the alloy after solution aging is composed of equiaxial primary  $\alpha$  phase and lamellar  $\beta$ -transformed structure.

### 1.2 Ballistic testing

To enhance the penetration resistance of titanium alloy plate, the heat-treated titanium plate was processed into a saw-tooth shape with an obliquity angle of  $60^\circ$  by wire electric discharge machining (WEDM), and the dimension is shown in Fig.2.

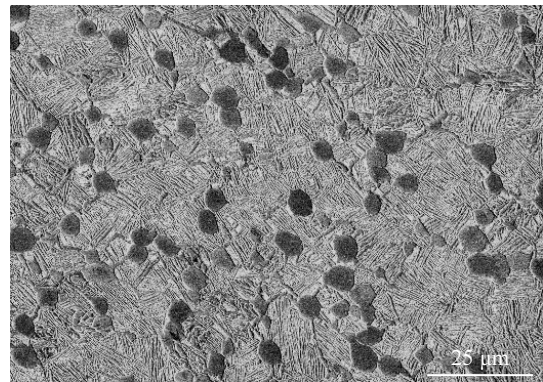


Fig.1 Microstructure of TC32 titanium alloy

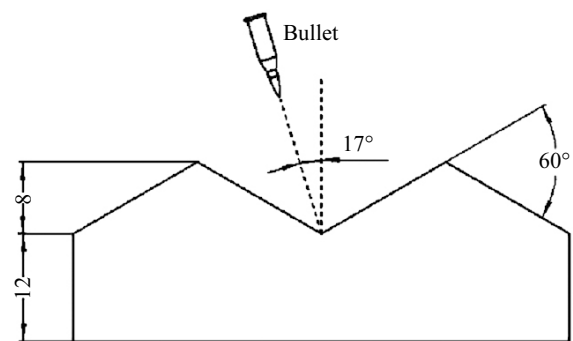


Fig.2 Diagram of target plate and bullet impact

According to the standard of GJB59.18-88, a 7.62 mm caliber ballistic gun was used as the test gun, and the 53 type WO-109C armor-piercing incendiary (API) was selected for this test. The hardness of the steel core was HRC63~65. The test distance and the shooting angle were 100 m and  $0^\circ$ , respectively. The speed of the projectile at 25 m from the muzzle was  $808_{-8}^{+7}$  m/s.

### 1.3 Microstructure characterization

After the ballistic testing, the center area was curved severely and the bullet left a crater on the target plate, the position of the projectile was deformed when the strain rate is about  $10^5 \text{ s}^{-1}$  [31,32]. The center of the crater was cut along the parallel direction to the incident direction of the projectile by WEDM.

The OM and SEM examination for the TC32 titanium alloy was carried out by using a Leica DMI 3000M and FEI NavaSEM450 SEM. Before the SEM and OM test, all observation areas were mechanically polished by automatic prototyping. The polishing solution is the OPS which was produced by Struers. The samples were etched in a solution of 10%HF, 7%HNO<sub>3</sub> and 83%H<sub>2</sub>O for optical microscope and SEM.

Due to the limited resolution of the SEM, especially the observation of the microstructure in the adiabatic shear band of the deformed titanium alloy, the FEI Titan-Themis TEM was used for observation. The focus ion beam (FIB) was used to prepare an accurate cut samples from the adiabatic shear band position, then the samples were thinned to about 40  $\mu\text{m}$  and soldered on a copper mesh. As shown in Fig.3a, the first sample was taken from the center of the ASB and matrix with FIB, the prepared sample is shown in Fig.3c. Fig.3b shows the second sample which was taken from the

tip region of crack in the ASB. It can be observed in Fig.3d that the sample prepared with FIB retains the crack tip region.

## 2 Results and Discussion

### 2.1 Macroscopic morphology of the crater

After the bullet impacts the TC32 titanium alloy target plate, the surface saw-tooth produces a strong obliquity effect. It can be clearly seen in Fig.4a that the bullet is embedded in the target at an angle of  $17^\circ$  from the normal direction. Although

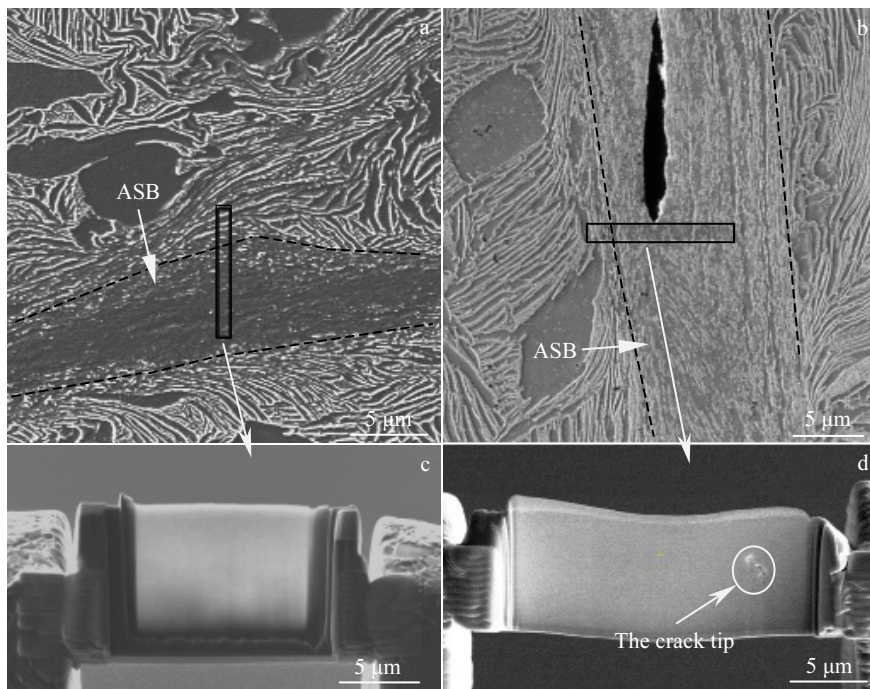


Fig.3 Preparation of TEM samples by FIB: (a, b) the sampling position of FIB (black box indicates the sampling position); (c, d) the TEM samples

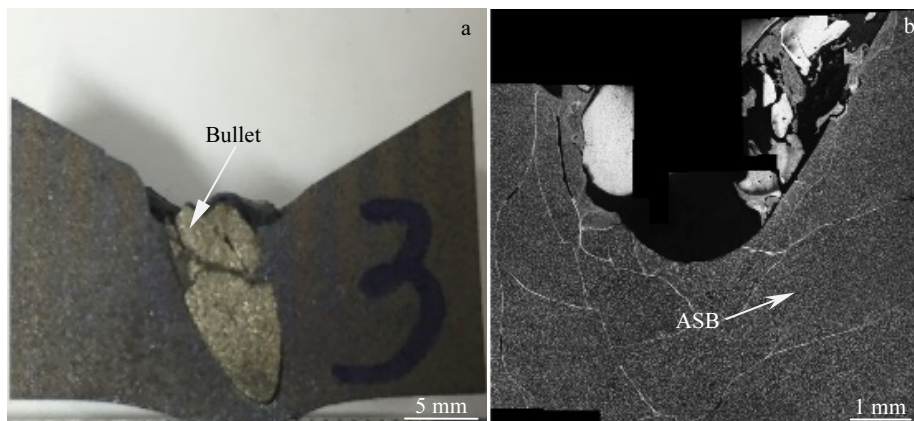


Fig.4 Crater profile (a) and microstructure of the crater profile (b)

it can produce obliquity effect, it is constrained by two bevels during the normalizing process and penetrates at the weakest part of the target plate. A convex shape can be observed on the back surface of the target plate, and cracks appear on the back of the target and are penetrated.

The TC32 titanium alloy target plate, after being impacted by the warhead at high speed, produces ASBs around the crater as shown in Fig.4b. It can be clearly seen that the ASBs are annularly distributed around the crater. As the distance from the crater increases, the annular band formed by the ASB gradually increases and is connected to the annular ring of the adiabatic shear band near the crater to form a net. This indicates that the formation and distribution of the adiabatic shear bands are consistent with the distribution of the shear stress formed after the bullet impacts the target plate in the local region. The ASB first forms at the portion where the shear stress is the greatest. This is consistent with Li's research results in the dynamic mechanical properties in relation to adiabatic shear band formation in titanium alloy-Ti17<sup>[33]</sup>.

## 2.2 Microstructural evolution behavior in ASBs

Fig.5 shows the TEM images from the matrix to the center of the ASB. It can be observed that the lath subgrains form

due to the shear stress. According to the selected area electron diffraction (SAED) analysis (Fig.5d), the elongated lath subgrains has  $\alpha$  titanium structure and evolve from  $\alpha$  phase in the matrix. In Fig.5a and Fig.5b, it can be observed that the width of the lath subgrain decreases from the outside to the center of the ASBs, and the dislocation density inside the subgrain increases as the deformation progresses. Under the influence of local temperature rise in ASB, the overall boundary energy can be reduced by dislocations movement, tangle and annihilate after rearrangement; lath subgrains collapse, boundaries form, and elongated subgrains break up. As can be seen in Fig.5c, the broken subgrains rotate to form approximately equiaxed recrystallized grains.

The width of the elongated lath subgrain is in the range of 100~200 nm, and the size of the formed equiaxed grain is also in the range of several hundred nanometers. This is consistent with the dislocation-corrected subgrain rotational dynamic recrystallization mechanism proposed by Meyers et al.<sup>[15,24,25]</sup>.

In order to analyze the formation of the cracks and the evolution of the microstructure, the sample was taken from the crack tip of ASB by FIB, and analyzed by TEM. Fig.6a is the bright-field image of the hole pattern formed at the crack tip, in which the gradient change of the microstructure can be

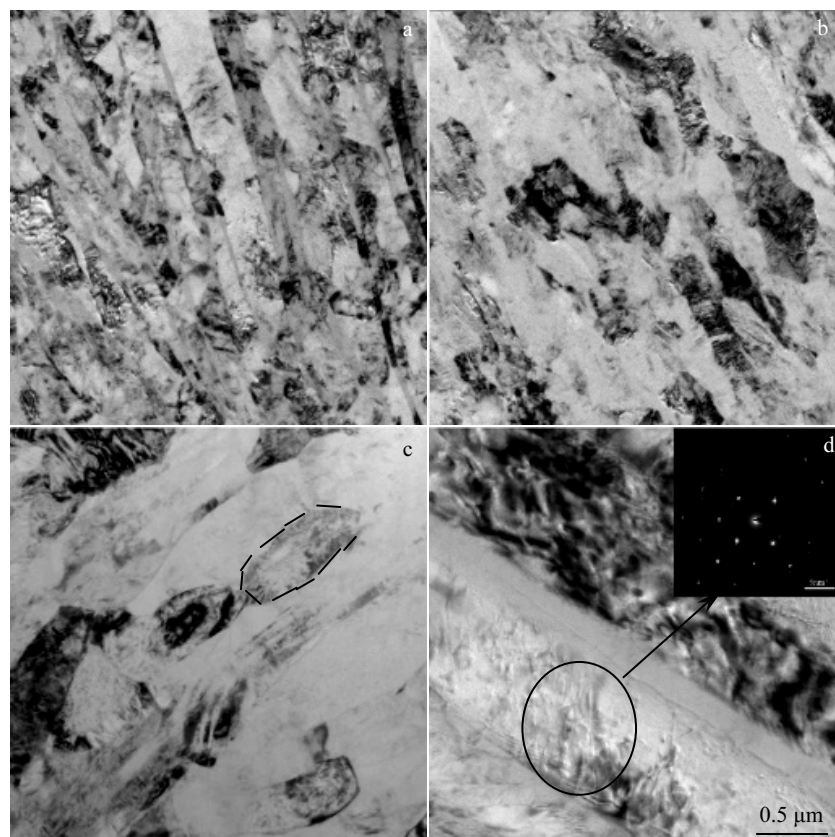


Fig.5 TEM images from the matrix to the center of the ASB: (a, b) the lath subgrain from the outside to the center of the ASB, (c) equiaxed recrystallized grains, and (d) the elongated lath subgrains and SAED pattern

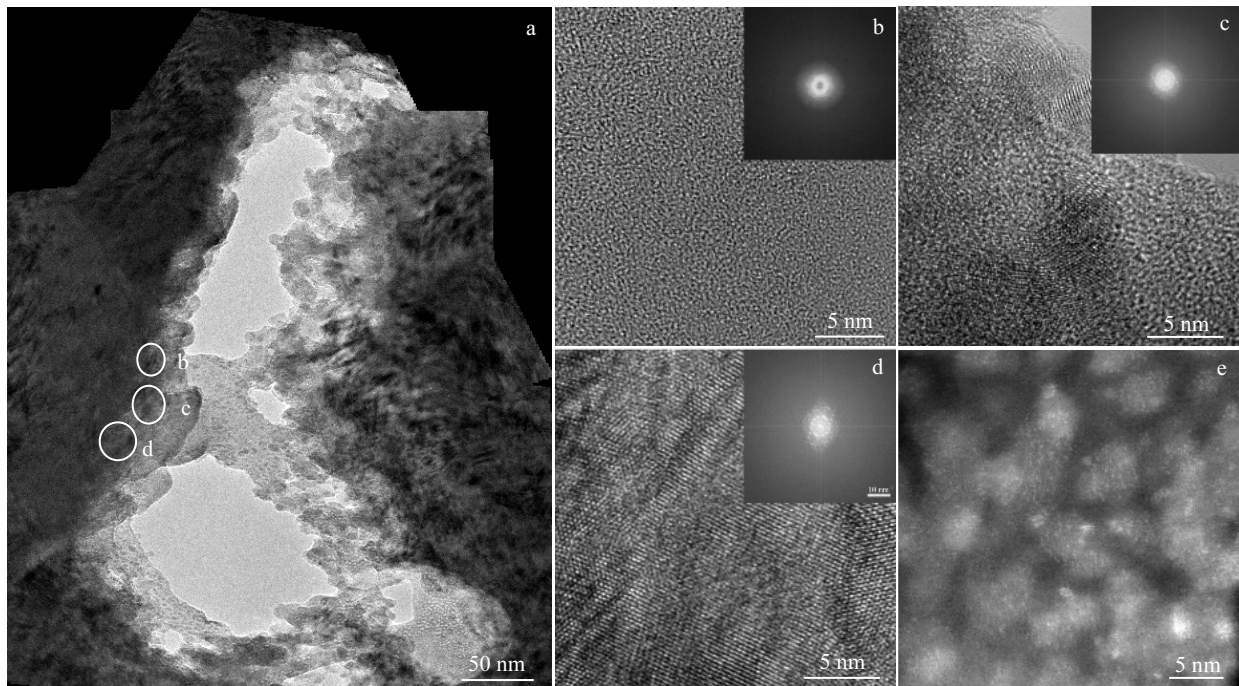


Fig.6 TEM images of the microstructures of an ASB: (a) hole pattern formed at the crack tip, (b) HRTEM image of a metallic amorphous state, (c) HRTEM image of amorphous-to-crystalline transition region, (d) nano-crystalline region, and (e) HAADF image of the nano-crystalline region

clearly observed. As shown in the bright area on left of the crack tip, there is almost uniform contrast. Fig.6b is the high-resolution transmission electron microscopy (HRTEM) image showing that the atoms are arranged in a short-range ordered with a typical metallic amorphous state. The Fourier-transformed diffraction pattern (as displayed from the amorphous scattering rings in the inset of Fig.6b) further confirms that there is no metallic crystal structure with long-range ordered structure in this region. The region adjacent to the amorphous region is a transition region between amorphous and crystalline. From Fig.6c, two different arrangements of long-range order and long-range disorder can be observed, and the diffraction pattern also includes the characteristics of two phases. Adjacent to the other side of the transition region is a nanocrystal region, and the grain size is in the range of several nanometers to 10 nanometers. The diffraction pattern (multiple sets of diffraction spots in Fig.6d) indicates that there are multiple grains in this range. Fig.6e shows the high-angle annular dark field (HAADF) image of this region, which is a Z-contrast image that can directly reflect the structural information of the sample. In this figure, the boundary and the size of nanocrystal grains can be clearly seen, further proving that the size range of nanocrystal grains is within 10 nanometers.

It is generally believed that the plastic instability in shear bands can lead to localized plastic flow. When the local heat

generation caused by plastic instability exceeds the heat conduction capacity of the matrix, the internal temperature of the ASBs rises sharply and can reach a higher temperature in a short time. Moreover, the temperature rise in different regions of the shear band will also be affected by stain. Assume that all the heat generated by plastic deformation is concentrated in ASBs at an ideal condition, the elevated temperature can be calculated by the following equation<sup>[34,35]</sup>.

$$\Delta T = \frac{\beta}{\rho C_v} \int_0^{\gamma} \tau d\gamma \quad (1)$$

where  $\rho$  is the density of the material ( $4.5 \text{ g/cm}^3$ ),  $C_v$  is the specific heat capacity ( $0.52 \text{ J}\cdot\text{g}^{-1}\cdot\text{K}^{-1}$ ),  $\tau$  is the shear stress,  $\gamma$  is the shear strain, and  $\beta$  is the Taylor-Quinney coefficient that characterizes the portion of the plastic deformation work converted into heat (assumed 0.9). The shear stress of TC32 titanium alloy is 700 MPa. Compared with the ASBs, the matrix grains do not undergo serious stretching and deformation. If most of the strain generated by deformation is concentrated in the ASB, the strain should be 11 by estimating the degree of overall deformation and the width of the ASBs.

The experiment was carried out at room temperature. The temperature rise in the ASB calculated from Eq.(1) is about 2962 K. The temperature in the ASB can reach 3260 K, far exceeding the melting point ( $T_m$ ) 1923 K of TC32. Fecht et al<sup>[36,37]</sup> found that metals can overheat at their melting points ( $T_m$ ) without melting and the highest overheating temperature

could be  $1.56 T_m$  (He) for its melting point. In this experiment, the estimated temperature in the ASBs is  $1.69 T_m$ , and has exceeded the superheat temperature, so melting will occur. The temperature rise will also be changed due to the different strain at the ASBs in different parts. After the high-speed deformation stops, no more heat is generated, and the temperature of ASBs will drop sharply and dissipate into the matrix. The extremely fast cooling rate is sufficient to directly change molten metal from liquid phase to amorphous phase; it is the reason why amorphous structure can be observed. The temperature distribution in ASBs is not uniform, and the cooling rate is also different, resulting in different microstructure in different locations. In the region where the cooling rate is relatively low, nano-crystals form. Both the temperature and cooling rate in ASBs are in a gradient distribution, resulting in a smooth transition from amorphous region to nanocrystal region. All these can prove that melting and rapid cooling processes have taken place in the ASBs. Meyers et al.<sup>[24]</sup> observed amorphous structure and nano-crystal in ASBs of steel, and they believed that the formation of nanocrystals was an evolution after rotational dynamic recrystallization. However, in this experiment, the strain or stress stored in the grains or sub-grain boundaries cannot break up the grains to form nano-crystals with a size below 10 nanometers, even less to induce amorphous phase. Fecht<sup>[36]</sup> proposed that solid materials can be deformed and overheated through plastic deformation, and then rapidly cooled to form amorphous. Li et al.<sup>[32]</sup> also believed that the occurrence of amorphous regions and nanocrystals is caused by melting and rapid cooling in the adiabatic shear bands. The above arguments and data analysis indicate that the theory of melting and fast quenching in ASBs is reasonable to explain the coexistence of the amorphous regions, amorphous-to-crystalline transition regions and fine-scale nanocrystalline region in these experimental conditions.

### 2.3 Initiation and propagation of cracks in adiabatic shear bands

The ASB is a local instability phenomenon caused by high strain rate deformation process. In the process of high strain rate deformation, the localization of plastic rheology in the adiabatic shear bands causes the temperature to rise sharply in a very short loading time, resulting in local thermal softening of the material. At the same time, material deformation will also produce strain hardening. Thermal softening and strain hardening are competitive relationships in the deformation process. In the process of high strain rate deformation, the heat generation rate caused by local plastic rheology exceeds its heat loss rate to surrounding metals, and the heat softening effect is greater than that of strain hardening, eventually forming cracks and causing shear instability. It is known that microvoids and microcracks get developed after the formation of ASBs. Timothy and Hutchings<sup>[29]</sup> proposed that the microvoids can nucleate in the center of the shear band, then

subjected to shear stress to grow and rotate, finally expand and join together to form the cracks. In this study, the formation of cracks in ASBs is consistent with the mechanism of microvoid nucleation, growth, and micro-rack formation. Different from the previous study of micro-crack nucleation in the center of adiabatic shear bands, the nucleation position of microvoid and the crack propagation position mostly appear between the deformed band of ASBs and matrix<sup>[38]</sup>. As shown in Fig.7a, the microvoids with circular or elliptical shape form at one side of the ASBs. All microvoids have smooth surfaces without second phase particles. It means that the material inside the band is quite soft and the temperature is high when the microvoids form. Many researchers such as Me-Bar and Shechtman<sup>[21]</sup>, Grebe et al.<sup>[39]</sup> reported that the formation of microvoids in shear bands was associated with thermal softening and local melting of the material in the shear band. This indicates that the strength at the interface is lower than that of the adjacent matrix due to the increasing of temperature at the moment of void formation, and nucleation occurs at the unevenness of the microstructure. As shown in Fig.7b, due to the complex effect of shear stress and tensile stress, the crack propagation changes its propagation direction across the ASB, and the crack propagation after the expansion will still extend along the interface. This further indicates that when the TC32 titanium alloy undergoes adiabatic shear

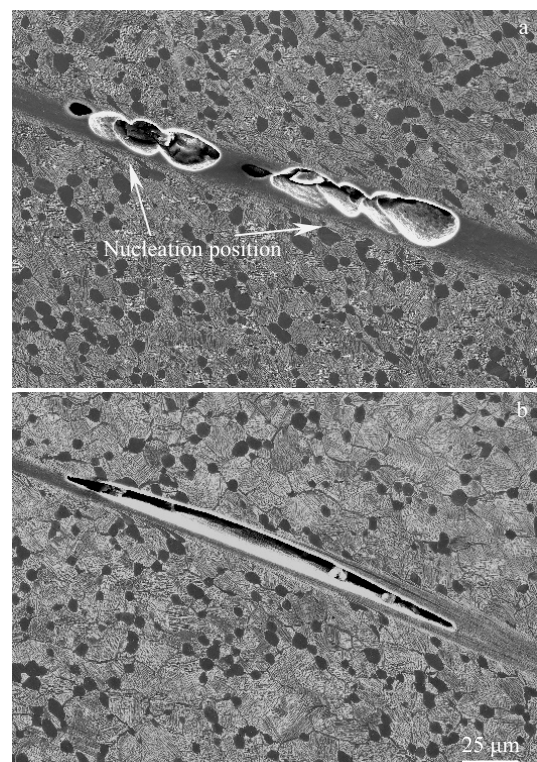


Fig.7 Microvoids (a) and cracks (b) in the adiabatic shear bands

failure in this experiment, the interface between the deformed band of ASBs and matrix is a weak position where microvoids and microcracks easily form.

By analyzing the evolution of the microstructure in the ASB, fine nanocrystalline and amorphous can form in the elongated ASB. Its organization is relatively uniform and the strength is high. At the same time, the matrix structure is also uniform and complete. This makes the interface between the deformed band of ASBs and matrix become a relatively weakened area and provides conditions for the formation of microvoids.

### 3 Conclusions

1) The equiaxed grain (100~200 nm) formation mechanism in ASBs produced in high-speed projectile impact experiment conforms to the dislocation-corrected subgrain rotational dynamic recrystallization mechanism.

2) The coexistence of the amorphous regions, the amorphous-to-crystalline transition regions, the fine-scale nano-crystalline region (<10 nm) are found in the crack tip analysis in the ASBs, which fully shows that melting and rapid cooling occur in ASBs during high-strain-rate deformation. The rationality of this conclusion is also proved by calculating the temperature rise in the shear band.

3) The initiation and propagation of cracks in the ASBs are mainly carried out along the transition region between the deformed band and matrix.

### References

- Song H, Wu G Q, Zhang Z G et al. *Materials Letters*[J], 2006, 60(28): 3385
- Wan Z P, Zhu Y E, Liu H W et al. *Materials Science and Engineering A*[J], 2012, 531: 155
- Zakaria M, Wu X. *Materials Science and Technology*[J], 2013, 21(2): 225
- Li Jianchong, Nan Hai, Zhao Jiaqi et al. *Rare Metal Materials and Engineering*[J], 2013, 42(6): 1105
- Zou D L, Luan B F, Liu Q et al. *Materials Science and Engineering A*[J], 2012, 558: 517
- Liu X, Tan C, Zhang J et al. *Materials Science and Engineering A*[J], 2009, 501(1-2): 30
- Peirs J, Tirry W, Amin-Ahmadi B et al. *Materials Characterization*[J], 2013, 75: 79
- Chichili R D, Ramesh K T, Hemker J K. *Journal of the Mechanics and Physics of Solids*[J], 2004, 52(8): 1889
- Wang B F, Yang Y. *Materials Science and Engineering A*[J], 2008, 473(1-2): 306
- Murr L E, Ramirez A C, Gaytan S M et al. *Materials Science and Engineering A*[J], 2009, 516(1-2): 205
- Yang Y, Wang B F. *Materials Letters*[J], 2006, 60(17-18): 2198
- Zhan H, Zeng W, Wang G et al. *Materials Characterization*[J], 2015, 102: 103
- Zhou F, Wright T, Ramesh K. *Journal of the Mechanics and Physics of Solids*[J], 2006, 54(7): 1376
- Xue Q, Meyers M A, Nesterenko V F. *Acta Materialia*[J], 2002, 50(3): 575
- Meyers M A, Xu Y B, Xue Q et al. *Acta Materialia*[J], 2003, 51(5): 1307
- Li Y S, Tao N R, Lu K. *Acta Materialia*[J], 2008, 56(2): 230
- Xu Y, Zhang J, Bai Y et al. *Metallurgical & Materials Transactions A*[J], 2008, 39(4): 811
- Mishra A, Richard V, Grégory F et al. *Materials Science and Engineering A*[J], 2005, 410-411: 290
- Murr L E, Trillo E A, Pappu S et al. *Journal of Materials Science*[J], 2002, 37(16): 3337
- Ran C, Chen P. *Materials*[J], 2018, 11(1): 76
- Me-Bar Y, Shechtman D. *Materials Science & Engineering*[J], 1983, 58(2): 181
- Andrade U, Meyers M A, Vecchio K S et al. *Acta Metallurgica et Materialia*[J], 1994, 42(9): 3183
- Meyers M A, Subhash G, Kad B et al. *Mechanics of Materials*[J], 1994, 17(2-3): 175
- Meyers M A, Chen Y J, Marquis F D S et al. *Metallurgical & Materials Transactions A*[J], 1995, 26(10): 2493
- Meyers M A, Nesterenko V F, Lasalvia J C et al. *Materials Science & Engineering A*[J], 2001, 317(1): 204
- Kad B K, Gebert J M, Perez-Pardo M T et al. *Acta Materialia*[J], 2006, 54(16): 4111
- Nesterenko V F, Meyers M A, LaSalviaab J C et al. *Materials Science & Engineering A*[J], 1997, 229(1-2): 23
- Timothy S P. *Acta Metallurgica*[J], 1987, 35(2): 301
- Timothy S P, Hutchings I M. *Acta Metallurgica*[J], 1985, 33(4): 667
- Timothy S P, Hutchings I M. *Journal of Materials Science Letters*[J], 1986, 5(4): 453
- Kurtaran H, Buyuk M, Eskandarian A. *Theoretical and Applied Fracture Mechanics*[J], 2003, 40(2): 113
- Li N, Wang Y D, Lin P R et al. *Acta Materialia*[J], 2011, 59(16): 6369
- Qiang L, Yongbo X, Bassim M N. *Materials Science and Engineering A*[J], 2003, 358(1-2): 128
- Mataya M C, Carr M J, Krauss G. *Metallurgical Transactions A*[J], 1982, 13(7): 1263
- Liu J, Li S, Zhou X et al. *Scripta Materialia*[J], 2008, 59(12): 1271
- Fecht H J. *Nature*[J], 1992, 356(6365): 133
- Fecht H J, Johnson W L. *Nature*[J], 1988, 334(6177): 50
- Zhou P, Guo W G, Su Y et al. *Journal of Materials Engineering and Performance*[J], 2017, 26(7): 3121
- Grebe H A, Pak H R, Meyers M A. *Metallurgical Transactions A*[J], 1985, 16(5): 761

## TC32 钛合金中高速弹丸冲击诱发绝热剪切带的组织演化行为

信云鹏, 朱知寿, 王新南, 李明兵, 刘格辰, 李 静, 商国强, 祝力伟

(中国航发北京航空材料研究院, 北京 100095)

**摘 要:** 采用光学显微镜 (OM), 扫描电子显微镜 (SEM) 和透射电子显微镜 (TEM) 研究了 Ti-5Al-3Mo-3Cr-1Zr 钛合金在高速弹丸冲击后的组织特征和演变行为。在弹坑周围, 绝热剪切带 (ASB) 和剪切应力一直呈半圆状分布。观察到绝热剪切带中尺寸较大等轴晶粒和细长板条亚晶粒的旋转细化过程。采用聚焦离子束 (FIB) 技术准确地从 ASB 中的裂纹尖端取样制备 TEM 样品, 在裂纹尖端区域周围发现非晶区、非晶-纳米晶过渡区、细小纳米晶区共存。计算结果表明, 绝热剪切带内温度升高可导致微观组织熔化, 快速淬火后形成非晶区和细小的纳米晶。由于绝热剪切带中的显微组织是细小的等轴晶和非晶, 具有较高的强度, 使变形带与基体之间成为相对较弱的区域, 绝热剪切带中的裂纹也主要在该区域萌生, 裂纹通过微孔洞旋转联结的方式扩展。

**关键词:** 绝热剪切带; 纳米晶; 非晶; TC32 钛合金

---

作者简介: 信云鹏, 男, 1991 年生, 博士, 中国航发北京航空材料研究院, 北京 100095, 电话: 010-62496635, E-mail: yunpengwhy@qq.com